PCCP

Accepted Manuscript

ROYAL SOCIETY OF CHEMISTRY

www.rsc.org/pccp

Experimental and Theoretical Studies on Aqueous-Phase Reactivity of Hydroxyl Radicals with Multiple Carboxylated and Hydroxylated Benzene Compounds

Prepared for Physical Chemistry Chemical Physics (PCCP)

Daisuke Minakata[1*]
Weihua Song[2]
Stephen P. Mezyk[3]
William J. Cooper[4]

1. Department of Civil and Environmental Engineering, Michigan Technological University, 1400 Townsend Drive, Houghton, MI, 49931.
2. Department of Environmental Science and Engineering, Fudan University, Shanghai, P.R. China.
3. Department of Chemistry and Biochemistry, California State University Long Beach, Long Beach CA 90840.
4. Department of Civil and Environmental Engineering, University of California, Irvine, CA 92697.

*Corresponding author. dminakat@mtu.edu, 906-487-1830

Abstract

In this study, we shed light on the initial addition of hydroxyl radicals (HO•) to multiple carboxylated and hydroxylated benzene compounds in aqueous-phase advanced oxidation processes (AOPs). We analyze the experimentally measured transient spectra near neutral pH using quantum mechanical-based time-dependent density functional theory (TD-DFT). The *ab initio* DFT method was first used to find and optimize aqueous-phase transition state structures, then the TD-DFT was used to analyze molecular orbitals (MOs) of the optimized transition state structures to reveal the functional groups that are responsible for the individual absorption peaks. The initial addition of HO• to the benzene ring produced hydroxycyclohexadienyl radicals. Then, HO-adducts are generated from dimerization or disproportionation of hydroxycyclohexadienyl radicals and represent their transient spectral peaks at approximately 350 nm and 250 nm. As reaction proceeds, the HO-adducts are decreased depending on the subsequent reactions. These investigations into the experimental transient spectra coupled with the theoretical analysis using the TD-DFT enable us to visualize an initial transformation of organic compounds induced by the aqueous phase HO• oxidation. Moreover, the experimental reaction rate constants and the theoretically calculated aqueous phase free energies of activation provide quantitative insights into the addition of HO• to multiple carboxylated and hydroxylated benzene compounds.

Introduction

Hydroxyl radicals (HO•) are electrophilic in nature and react with electron-rich sites of organic compounds by complex reaction mechanisms involving free radicals. In the aqueous-phase, advanced oxidation processes (AOPs) generate HO• at ambient temperature and atmospheric pressure,[1,2] and in many cases HO• can transform parent organic compounds into low molecular weight biodegradable carboxylic compounds.[3] AOPs are used in drinking water treatment,[4,5] water reclamation,[6] and industrial wastewater treatment processes.[7,8] In natural aquatic environments, the photolysis of natural organic matter (NOM)[9,10] and effluent organic matter (EfOM) from wastewater discharge[11] at the surface of the water indirectly generates HO•, which again contributes to the fate and transformation of contaminant chemical compounds.[12] In a water droplet in the atmosphere HO• are generated via nitrite and nitric acid,[13] and are involved in the atmospheric aqueous-phase chemical oxidation of anthropogenic carbon and nitrogen, and in aerosol formation.[14] Under physiological conditions, HO• are important intermediates for the reactive oxygen species that cause cell damage.[15, 16]

A number of previous studies have revealed the major reaction mechanisms of HO• in the aqueous phase.[13, 17] These mechanisms include: 1) H-atom abstraction from C-H bonds in aliphatic compounds; 2) HO• addition to unsaturated carbons of alkenes and aromatic compounds, and 3) HO• interactions with S-, N-, or P-containing compounds.[17] Minakata *et al*. developed a comprehensive group contribution method (GCM) that was able to predict the reaction rate constants of more than 500 reactions of HO• with organic compounds using parameters determined from experimental values that represent the chemical reactivity and contributions of functional groups.[18] The GCM predicts the aqueous-phase HO• rate constants within a factor of 2.

Among the vast number of organic compounds, benzene compounds are an important group of compounds for reactions with HO• in water. Benzoic acid, its dissociated form benzoate, and benzene rings with multiple hydroxyl and carboxylate functional groups appear in NOM,[19, 20] pharmaceutical and personal care products,[21] and engineered nanomaterials.[22] The hydroxyl group donates electron density to

the active sites (i.e., C-H and C=C bonds) of organic compounds, and hence, enhances the reactivity of HO•. The carboxylic or carboxylate functional groups are hydrophilic, producing hydrogen bonds with water molecules. Because of their strong electron-withdrawing effect, these functional groups decrease the overall reactivity of HO• with organic compounds. The calculated functional group contribution factors for carboxylic and carboxylate functional groups in the GCM are 0.043 and 0.184, respectively, for H-atom abstraction from the C-H bond, and 0.234 for HO• addition to a benzene ring with a carboxylic functional group. These values represent a strong electron withdrawing effect (note that the smaller group contribution factors indicate stronger electron withdrawing effects) relative to other groups (e.g., 0.200 for Cl, 0.119 for F, 0.154 for CO) for H-atom abstraction and are consistent with the Taft constants for aliphatic compounds and the Hammet constants for aromatic compounds.[18] **Error! Bookmark not defined.**

Although the second-order reaction rate constants describe the general reactivity of HO•, examining how functional groups affect the reactivity of HO• in different organic compounds is challenging. In experiments, we measure a reaction rate constant that combines the reaction rates of all of the elementary reactions in which HO• participates. In addition to absolute kinetics, transient spectra that represent the ultraviolet-visible (UV-VIS) absorbance for these short-lived radicals/products generated by the reactions with HO• also can be readily determined. Although these transient spectra contain information critical to the observed chemical reactivity, transformation, and stability, this information has been under-utilized to investigate aqueous-phase chemical reactions in depth. When numerous active sites/functional groups are present in the molecule, the transient spectrum represents synergic effects. Therefore, experimental investigations only generate, but do not typically attempt to analyze, these spectra.

Computational chemistry can be used to probe chemical reactivity and to analyze the changes in the electronic properties of the reactants, transition states, and products as a reaction proceeds. The dramatic improvement in computational power, and the development of sophisticated computational

chemistry suites with robust implicit solvation models, makes it now possible to analyze aqueous-phase chemical reactions. Minakata and Crittenden[23] developed linear free energy relationships (LFERs) that relate experimentally observed rate constants with the aqueous-phase free energies of activation for H-atom abstraction from the C-H bonds and HO• addition to an unsaturated alkene carbon atoms in molecules. This approach was further developed for haloacetates to investigate their changes in the electrostatic potential and charges throughout the reaction process[24], and then extended to the subsequent radical reactions (i.e., molecular oxygen addition to carbon-centered radicals, uni-molecular and disproportionation of peroxyl radicals) after the reactions of HO•.[25] Nevertheless, there are few applications of computational chemistry to aqueous phase chemical reactions involving HO•.[26]

Time-dependent density functional theory (TD-DFT)[27] is robust computational technique that enables us to investigate into the TD excited state electronic structures of various chemical compounds under different physical chemical processes (e.g., ultraviolet-visible spectroscopy, nonlinear optics, and photochemistry). Successful application of the TD-DFT includes: 1) photovoltaic performance[28]; 2) dye chemistry[29]; 3) electron transfer chemical reactions[30], and 4) spectroscopic investigations on transition metal complexes[31]. TD-DFT makes it possible to examine the TD molecular orbitals (MOs) and associated structural changes in chemical reactions.

Here we investigated aqueous-phase HO• reaction with multiple carboxylated and hydroxylated benzene compounds. The coupling of experimental measurements and theoretical investigations reveals how the carboxylate and/or hydroxyl functional groups affects the aqueous-phase chemical reactivity of HO• by determining the kinetic rate constants, thermochemical properties, and transient spectra.

Materials and Methods

Pulse radiolysis experiments

Electron pulse radiolysis experiments were conducted at the Notre Dame Radiation Laboratory using their 8-MeV Titan Beta model TBS-8/16-1S linear accelerator.[32] This pulse radiation and transient absorption detection system have been previously described in detail.[33] Dosimetry was performed with

N_2O-saturated solutions of 1.00×10^{-2} M KSCN solutions at $\lambda = 472$ nm, ($G\varepsilon = 5.2 \times 10^{-4}$ m^2 J^{-1}) with average doses of 3-5 Gy per 2-4 ns pulse. All experimental data were determined by averaging 12 to 15 replicate pulses in continuous flow mode.

The radiolysis of water is described in equation 1:[17]

$$H_2O \rightsquigarrow (0.28)\ HO\bullet + (0.06)\ H\bullet + (0.27)\ e^-_{aq} + (0.05)\ H_2 + (0.07)\ H_2O_2 + (0.27)\ H^+ \quad (1)$$

where the numbers in parentheses are the G-values (yields) in units of μmol J^{-1}. To study only the reactions of the HO• with multiple carboxylated and hydroxylated compounds, the solutions were pre-saturated with nitrous oxide (N_2O), which quantitatively converts the hydrated electrons and hydrogen atoms to HO• via the reactions[17]:

$$e^-_{aq} + N_2O + H_2O \rightarrow N_2 + HO^- + HO\bullet \qquad k_2 = 9.1 \times 10^9\ M^{-1}\ s^{-1} \quad (2)$$

$$H\bullet + N_2O \rightarrow HO\bullet + N_2 \qquad k_3 = 2.1 \times 10^6\ M^{-1}\ s^{-1} \quad (3)$$

All multiple carboxylated and hydroxylated benzene compound solutions were prepared in solution in the range of 0.5 to 1.0 mM. The solutions were adjusted to pH 6.9 to 7.1 using both 5.0 mM phosphate buffer and perchloric acid or sodium hydroxide. The reaction of HO• with phosphate has a negligible contribution to the rate constant being approximately five orders of magnitude lower than those for the benzene compounds.

Quantum mechanics-based ab initio theoretical calculations

All *ab initio* quantum mechanical calculations were performed with Gaussian 09 revision D.02[34] using the Michigan Tech high performance cluster "Superior" unless otherwise specified. The electronic structures of the molecules and radicals in the ground and transition states were optimized using density functional theory (DFT) at the level of M06-2X/Aug-cc-pVDZ[35] with the implicit SMD solvation model.[36] This approach was successfully applied to examining the HO• reactions with the single-functional benzene compounds in the aqueous-phase.[25] The transition state was verified by an imaginary frequency factor. Once the electronic structures were optimized, the frequencies determined from the optimization were used to calculate the aqueous-phase free energy of activation, $\Delta G^{act}_{aq,calc}$, and the

volume of molecules or radicals using the same DFT method and level of basis set. Theoretically calculated absorption spectra in the UV-VIS wavelength range were obtained from a TD-DFT analysis[37] of the optimized aqueous phase transition state structure at the level of M06-2X/cc-pVQZ and wB97XD/cc-pVQZ with the SMD solvation model. The TD-DFT contained 20 singlet and 20 triplet-excitation states. To investigate the contributions from MOs to the peak of the UV-VIS spectra, MOs were determined using a natural population analysis (NPA) at the level of M06-2X/cc-pVQZ with the SMD solvation model based on the optimized structure obtained at the level of M06-2X/Aug-cc-pVDZ with the SMD solvation model.

Results and Discussions

Overall results for HO• addition to various multiple carboxylated benzene compounds

Table 1 shows the overall results for the addition of HO• to carboxylated and hydroxylated benzene compounds and includes the experimental HO• reaction rate constants and the theoretically calculated $\Delta G^{act}_{aq,calc}$, in kcal/mol. When the $\Delta G^{act}_{aq,calc}$ values are negative, increasing the temperature causes a decrease in the reaction rate constant, which have seen in various nonintuitive phenomena (e.g., protein folding kinetics[38]). In these circumstances, the forward reaction is energetically favored by overcoming the transition state but the entropy of the reaction is not favored with respect to the reactants. We have observed negative $\Delta G^{act}_{aq,calc}$ values for the aqueous phase HO• addition to aromatic compounds with various single-functional groups and successfully developed the LFER for this class of compounds as:

$$\ln k_{chem} = -0.14\, \Delta G^{act}_{aq,calc} + 20.30 \quad (n = 15) \qquad (4)$$

where k_{chem} = chemical reaction rate constant that is determined, from the overall experimental rate constant.[25] The experimental overall reaction rate constant, k, can be expressed as in eq 5:[39]

$$k = \frac{k_D k_{chem}}{k_D + k_{chem}} \quad (5)$$

k_D is the diffusion-limited rate constant. This k_D value was calculated using Smoluchowski's equation[40] in eq 6:

$$k_D = 4\pi D_l r N_0 / 1000 \quad (6)$$

where D_l is the aqueous-phase diffusion coefficient for the solute and radical (i.e., reactants), cm^2/s, r is the sum of radius for reactants, Å, and N_0 is Avogardo's number. The diffusion coefficient of small molecules and radicals in the aqueous-phase can be calculated using the Hayduk-Laudie correlation[41] as shown in eq 7:

$$D_l = \frac{13.26 \times 10^{-5}}{\left(\mu_\varpi\right)^{1.14} \left(V_b\right)^{0.589}} \quad (7)$$

where μ_ϖ is the viscosity of water, cP, (1 kg/m·s = 1000 cP), and V_b is the molar volume of the solute at the temperature at which a liquid boils at 1 atm of pressure, cm^3/mol.

The LFER determined for only HO• reaction with multiple carboxylated and hydroxylated benzene compounds in this study is:

$$\ln k_{chem} = -0.19\ \Delta G^{act}_{aq,calc} + 21.09\ (n = 14) \quad (8)$$

as shown in Figure 1 with the individual parameters for the kinetics and diffusion coefficients summarized in Table 1. There was difficulty in convergence for the transition state structure optimization and we were not able to find the optimized transition state structures for pyromellitic acid and 1,2,3,4,5-pentacarboxylic acid. There is little difference observed between these two LFER expressions in eqs 4 and 8; however, the LFER established for the multiple carboxylated and hydroxylated benzene compounds has a slightly larger slope. When there were several positions available for the addition of HO• to the benzene ring, the overall $\Delta G^{act}_{aq,calc}$ was calculated using the Benson's thermochemical additivity principle[42] (i.e., $\Delta G^{act}_{aq,calc} = \sum_i \Delta G^{act(i)}_{aq,calc}$, where i = the position where HO• was added). The

summation might have caused the slight differences in the slope. Nevertheless, the observed linear correlation may be used to predict the rate constants given that there are limitations of calculating the aqueous-phase second order reaction rate constants (accuracies of ±0.5 kcal/mol of the $\Delta G^{act}_{aq,calc}$ values are required to calculate the rate constant within the difference of factor of 2 according to the transition state theory[43]) directly. Detailed discussions of each reaction mechanism will be given in the following sections.

(Table 1 goes here)

Overall experimental and calculated results for the addition of HO• to the hydroxylated and carboxylated benzene compounds including the literature reported values such as Ashton et al. (1995)[44] and Wander et al. (1968)[45] for benzoic acid, Kwon et al. (2009)[46] for benzoate and Charbouillot et al. (2011)[47] for terephthalic acid.

(Figure 1 goes here)

Linear Free Energy Relationships between experimental rate constants for the chemical reactions, k_{chem}, and theoretically calculated $\Delta G^{act}_{aq,calc}$. The error bar indicates the range of the literature reported values.

Hydroxyl radical with benzoate and benzoic acid

Measured transient absorption spectra provide mechanistic insights into the TD structural changes from the reactants to the molecular transition state. For example, Figure 2 indicates the time-dependent transient spectra for the reaction of HO• with benzoate in the aqueous-phase. Experimental transient spectra were obtained at reaction times of 1, 5, 50, and 100 µsec, at pH of 6.9. The transient spectra indicate that the absorbance has a peak at approximately 330 nm and is seen to decrease as the reaction proceeds. This significant decrease of the transient spectra after 100 µsec of reaction at both around 320 nm and 340 nm indicates that the hydroxycyclohexadienyl radical that is generated by the HO• reaction with benzoate is being transformed into another product of radicals. This product in the N_2O-saturated solution of this experiment is expected to be a higher molecular weight species resulting from the

dimerization or disproportionation of hydroxylcyclohexadienyl radicals as was postulated by the product study for benzene compound.[48] Simic et al. (1973)[49] investigated the reaction of HO• with benzoate at pH of 9.2 and obtained a peak maximum at 330 nm with a corresponding molar absorptivity of 3,800 M^{-1} cm^{-1}, consistent with our experimental findings.

(Figure 2 goes here)

Experimental transient absorption spectra for the reaction of HO• with benzoate

The theoretical calculations found and optimized the transition state structures for ortho, meta, and para addition of HO• to benzoate, respectively. The TD-DFT analysis at the level of M06-2X/cc-pVQZ revealed that the addition of HO• at the ortho and para positions of benzoate were associated with the peaks at wavelengths, λ_{max}, of 322 nm and 324 nm, respectively, close to the peak of the measured transient spectra at 330 nm. In contrast, the addition of HO• at the meta position showed two peaks at wavelength, λ_{max} of 326 nm and 246 nm. To determine what MOs contribute to the different excited states of the transition state radicals, we first calculated the energies for the lowest unoccupied molecular orbital (LUMO)+1, LUMO, singly occupied molecular orbital (SOMO), and SOMO-1 orbitals. For calculating these energies of MOs, we applied the TD-DFT at the levels of wB97XD/cc-pVQZ and M06-2X/cc-pVQZ with the SMD solvation model. The wB97XD functional is known to contain empirical dispersion functions[50] and Wielopolski et al. (2014) successfully evaluated the lowest excited energy for various dye molecules using this functional.[28] We found the consistencies of energies calculated between these two methods. Table 2 summarizes the SOMO-LUMO gap, energies at the lowest excited state, and the oscillator strength (i.e., contribution of each MO to the excitation). The specific energies for LUMO+1, LUMO, SOMO, and SOMO-1, and energies at the λ_{max} are summarized in Table S1 of supporting information. For the HO• addition at the benzoate ortho-position, the energy at the lowest excited state was calculated as 2.7 eV at the level of M06-2X/cc-pVQZ, which is close to the energy difference (i.e., 2.4 eV) between SOMO-1 and SOMO for the alpha-spin. In comparison, the energy gap between SOMO and LUMO was 6.9 eV. Accordingly, the excitation from SOMO-1 to SOMO is a major

driving factor for the excitation at the lowest state. The same contribution is also observed for the meta- and para-position additions. Then, we investigate the contributions from MOs to the peak of the UV-VIS spectra (Figure 3). The SOMO and SOMO-1 for the additions at both ortho and para positions indicate that these orbitals are localized on the carboxylate functional group, whereas the LUMO shows the localization on the hydroxyl group of hydroxycyclohexadienyl radicals that were generated by the addition of HO•. The electron withdrawing effect of the carboxylate functional group promotes a spatial localization of LUMO on the hydroxyl group and a decoupling from the SOMO. This decoupling decreases of the transient spectra at around 340 ~ 350 nm of wavelength. The LUMO+1 for both ortho and para positions show the localization of these orbitals on the hydroxycyclohexadienyl radicals. In contrast, the delocalized SOMO-1, SOMO, LUMO, and LUMO+1 throughout the entire structure for the addition at the meta-position contribute more significantly to the decrease of the transient spectra at around 320 nm.

(Table 2 goes here)

The SOMO-LUMO energy gap calculated at the level of wB97XD/cc-pVQZ and M06-2X/cc-pVQZ. Values in () are by M06-2X/cc-pVQZ. The lowest excited state with the MO contributions calculated at the level of M06-2X/cc-pVQZ for the aqueous-phase reaction of HO• with benzoate

(Figure 3 goes here)

Molecular orbitals of SOMO-1, SOMO, LUMO, and LUMO+1 for the aqueous-phase reaction of HO• with benzoate

Hydroxyl radical addition to multiple carboxylated benzene compounds

We extended both the experimental and theoretical investigations to multiple carboxylated benzene compounds such as phthalic acid (1,2-dicarboxylic acid), terephthalic acid (1,4-dicarboxylic

acid), trimesic acid (1,3,5-tricarboxylic acid), pyromellitic acid (1,2,4,5-tetracarboxylic acid), and 1,2,3,4,5-pentacarboxylic acid. As shown in Table 1, the overall experimental reaction rate constants decreased as the number of carboxylate functional groups increased. The theoretically calculated $\Delta G^{act}_{aq,calc}$ values indicated that the position and number of carboxylate functional groups on the benzene ring significantly affect the reactivity of HO•. For example, the addition of HO• to phthalic acid at the 3 position corresponds to a $\Delta G^{act}_{aq,calc}$ of -4.85 kcal/mol, whereas a $\Delta G^{act}_{aq,calc}$ of -3.00 kcal/mol was required for addition at the 4 position. This difference indicates that the steric effects from the carboxylate functional group are less significant than the resonance effect for the addition of HO• to phthalic acid. For terephthalic acid, the required $\Delta G^{act}_{aq,calc}$ for the addition of HO• at any position was -7.61 kcal/mol, which is much smaller than the values for phthalic acid. When three carboxylate functional groups are on the benzene ring at the 1, 3, and 5 positions, the $\Delta G^{act}_{aq,calc}$ was -6.12 kcal/mol for the addition of HO• at the 2, 4, or 6 position. Only one reaction rate constant of HO• with terephthalic acid, $(4.0 \pm 0.1)\times10^9$ $M^{-1}s^{-1}$, has been reported in the literature[47], consistent with our experimental value of $(4.95 \pm 0.28)\times10^9$ $M^{-1}s^{-1}$.

Coupling the measured transient spectra for the addition of HO• to multiple carboxylated benzene compounds (Figure 4) with the theoretically calculated MOs (Figure 5) and associated energies (Table 3) show how the positions and number of carboxylate functional groups affect the addition of HO•. The measured transient spectra (Figure 4) for phthalic acid, terephthalic acid, trimesic acid, pyromellitic acid, and 1,2,3,4,5-pentacarboxylic acid in neutral pH solution showed two major peaks at approximately 350 nm and 250 nm. More carboxylate functional groups blue-shifted the λ_{max} toward 400 nm. Analysis of the MO contribution (Figure 5) indicates the localization of the molecular orbitals on one of carboxylate functional groups at both levels of SOMO and SOMO-1 for all the multiple carboxylated benzene compounds, as observed for the benzoate. The LUMO and LUMO+1 orbitals are localized on either the hydroxyl group of the hydroxycyclohexadienyl radicals. The analysis of the MO also revealed

that the excited state is LUMO at around 350 nm, whereas the combinations of various SOMO and LUMO contribute to the peak at around 250 nm. This different orbital contributions are supported by the fact that the transient spectral peaks at around 260 nm for terephthalic acid, pyromellitic acid and 1,2,3,4,5-pentacarboxylic acid are fewer in number than those for phthalic acid and trimesic acid. The terephthalic acid, pyromellitic acid, and 1,2,3,4,5-pentacarboxylic acid produce symmetric hydroxycyclohexadienyl radical structures regardless of the position of HO• addition. In contrast, the asymmetric structures of hydroxycyclohexadienyl radicals are generated from phthalic acid and trimesic acid (e.g., 3-hydroxy and 4-hydroxy cyclohexadienyl radicals for phthalic acid). We did not observe a significant decrease in the transient spectra in reaction times between 1 μsec to 100 μsec for the reaction of HO• with the multiple carboxylated benzene compounds. This result most likely occurred because more stable transients of HO-adducts were generated from the slower reaction of HO• with the multiple carboxylated benzene compounds than with benzoate or benzoic acid.

The theoretically calculated energies of various excited states indicate that the energy gaps between SOMO and LUMO for the multiple carboxylated benzene compounds (i.e., 5.5~6.8 eV) are smaller than those for the singly carboxylated compounds (i.e., 6.2~7.1 eV), which indicate the slower kinetics due to synergic effect of electron-withdrawing ability of multiple-carboxylate functional groups. The analysis on wavelength, energy, and the fraction at the lowest excited state for the multiple carboxylated benzene compounds vary by the compounds and the position of HO• addition.

(Table 3 goes here)

The SOMO-LUMO energy gap calculated at the level of wB97XD/cc-pVQZ and M06-2X/cc-pVQZ. Values in () are by M06-2X/cc-pVQZ. The lowest excited state with the MO contributions calculated at the level of M06-2X/cc-pVQZ for the addition of HO• to multiple carboxylated benzene compounds.

(Figure 4 goes here)

Experimental transient spectra for the addition of HO• to multiple carboxylated benzene compounds

(Figure 5 goes here)

Theoretically calculated MOs for the addition of HO• to multiple carboxylated benzene compounds

Hydroxyl radical addition to multiple hydroxylated benzene compounds.

To investigate the effect of hydroxyl functional groups in benzoate compounds, we investigated the HO• addition to: 1) mono-hydroxylated benzoic acid such as salicylic acid (2-hydroxybenzoic acid), 3-hydroxybenzoic acid, and 4-hydroxybenzoic acid; 2) di-hydroxybenzoic acids (2,3-, 2,4-, 2,5-, and 2,6-dihydroxybenzoic acids), and 3) tri-hydroxybenzoic acids (2,3,4- and 3,4,5-trihydroxybenzoic acids) near neutral pH. Figure 6 shows the TD transient spectra, Figure S1 of supporting information shows the MOs for the excited states, and Table 4 shows the associated excited-state energies for the reactions of HO• addition to multiple hydroxylated benzoic acids at various positions.

(Tables 4 goes here)

The SOMO-LUMO energy gap calculated at the level of wB97XD/cc-pVQZ and M06-2X/cc-pVQZ. Values in () are by M06-2X/cc-pVQZ. The lowest excited state with the MO contributions calculated at the level of M06-2X/cc-pVQZ for the reactions of HO• addition to multiple hydroxylated benzoic acids

(a) Excited state energies for the reactions of HO• addition to salicylic acid at 3-, 4-, 5-, and 6-positions

(b) Excited state energies for the reactions of HO• addition to 3-hydroxybenzoic acid at 3-, 4-, 5-, and 6-positions

(c) Excited state energies for the reactions of HO• addition to 4-hydroxybenzoic acid at 2- and 3-positions and to 2,3-dihydroxybenzoic acid at 4-, 5-, and 6-positions

(d) Excited state energies for the reactions of HO• addition to 2,4-dihydroxybenzoic acid at 3-, 5-, and 6-positions and to 2,6-dihydroxybenzoic acid at 4- and 5-positions

(e) Excited state energies for the reactions of HO• addition to 2,5-dihydroxybenzoic acid at 3-, 4-, and 6-positions and to 3,4-dihydroxybenzoic acid at 2- and 5-positions

(f) Excited state energies for the reactions of HO• addition to 2,3,4-trihydroxybenzoic acid at 5- and 6-position, and to 3,4,5-trihydroxybenzoic acid at 2- or 6-position

(Figure 6 goes here)

Time-dependent transient spectra for the reaction of HO• with multiple hydroxylated benzoic acids

As shown in Table 1, the overall experimental reaction rate constants for all the hydroxylated benzoic acids are larger than those for the multiple carboxylated benzene compounds examined above. Electron-donating hydroxyl functional group(s) significantly enhance the overall reactivity of HO•. It is noted that we did not consider a hydroxyl proton assisted electron transfer from the hydroxyl functional groups to HO• in the $\Delta G^{act}_{aq,calc}$ calculations. This is because the hydroxyl functional group forms a hydrogen bond with surrounding water molecule(s) and the past experimental observations on the reactions between aliphatic alcohol compounds and HO• indicated that this electron transfer was negligible in the aqueous phase.[51] The experimental rate constants for the di-hydroxybenzoic acids are larger than those for the tri-hydroxybenzoic acids. This is attributed to the entropy term being more dominant in the $\Delta G^{act}_{aq,calc}$ for the tri-hydroxybenzoic acids than for the di-hydroxybenzoic acids, and therefore, less negative $\Delta G^{act}_{aq,calc}$ values were obtained. The $\Delta G^{act}_{aq,calc}$ values for all the hydroxybenzoic acids fell in the close range from -13.0 kcal/mol to -18.0 kcal/mol except for salicylic acid (-23.4 kcal/mol). To investigate the differences in the chemical reactivity with HO•, we analyzed the experimental transient spectra and calculated the MOs that contribute to the associated transient peak. An introduction of hydroxyl functional group(s) on the benzoic acids indicates additional transient peaks that have not been observed for the multiple carboxylated benzene compounds. For example, the transient spectra for salicylic acid shows a broad peak at around 380 nm in addition to the two transient peaks that were observed for carboxylic and 1,2-dicarboxylic benzoic acids at around 260 nm and 340 nm, respectively. The analysis of MO using the TD-DFT revealed that the transient peak around 380 nm is

associated with the LUMO of the 4-hydroxy-cyclohexadienyl radical generated from the HO• addition to the salicylate at the 4-position (Figure 7). The other two peaks were found to be correlated with the MO from the hydroxyl functional group of the hydroxycyclohexadienyl radicals. We also found the additional transient peak at around 300 nm for the HO• addition to the 4 hydroxybenzoic acid. Similarly, we found additional transient peak that associates with the LUMO and LUMO+1 for the other hydroxylated benzene compounds. In these circumstances, the excited MOs are mainly localized on the hydroxyl functional group of hydroxycyclohexadienyl radicals. The wavelength that is responsible for the additional transient peak varies by the compounds and the structure of the associated hydroxycyclohexadienyl radicals.

(Figure 7 goes here)

Theoretically calculated MO for the addition of HO• to the salicylic acid

One distinctive difference in the observed reactivity for HO• addition to the multiple hydroxylated benzene compounds is the stability of the HO-adduct generated from the hydroxycyclohexadienyl radicals. As compared to the TD decrease in the transient spectra for the HO• addition to the multiple carboxylated benzene compounds, the HO-adduct showed a significant decrease of the TD transient spectra at specific wavelength. These differences are consistent with faster decay kinetics for the hydroxylated benzene compounds, the larger observed rate constants, the smaller $\Delta G^{act}_{aq,calc}$ values, and the larger energy gap between SOMO and LUMO observed in Tables 4.

Conclusions

In this study, we investigated into the initial addition of HO• to multiple carboxylated and hydroxylated benzene compounds by the pulse radiolysis technique and the TD-DFT based theoretical calculations. The M06-2X/Aug-cc-pVDZ with the implicit SMD solvation model was successfully applied to find and optimize the transition state structures for the addition of HO• on the benzene rings and calculate the aqueous-phase free energies of activation. The LFER that relate the experimentally

determined HO• chemical reaction rate constants and the aqueous phase free energies of activation was developed as: $\ln k_{chem} = -0.19\ \Delta G^{act}_{aq,calc} + 21.09$ (n = 14). The experimental transient spectra and the TD-DFT analysis on the UV-VIS spectra and the MOs enabled us to visualize an initial transformation of hydroxycyclohexadienyl radicals induced by the aqueous phase HO• and stability of the HO-adduct generated from the hydroxycyclohexadienyl radicals. It was found that the excited state of hydroxyl group of cyclohexadienyl radicals contributed to the transient spectral peak at around 350 nm. The analysis of the MO revealed that the excited state is LUMO at around 350 nm, whereas the combinations of various SOMO and LUMO contribute to the peak at around 250 nm. The MOs analysis also indicated the localization of the MOs on one of carboxylate functional groups at both levels of SOMO and SOMO-1, and the LUMO and LUMO+1 orbitals are localized on either the hydroxyl group of the hydroxycyclohexadienyl radicals.

Acknowledgement

DM appreciates support from the Michigan Tech HPC cluster "Superior". The authors appreciate the use of the accelerator facilities at the University of Notre Dame Radiation Laboratory, which is supported by Department of Energy. WJC and WS appreciate support from NSF CBET-1034555.

References

[1] W.H. Glaze, Environ. Sci. Technol. 1987, **21**, 224.

[2] W.H. Glaze, J.W. Kang, J.AWWA. 1988, **80**, 57.

[3] J. R. Bolton, S. R. Carter, Chap. 33, in G. R. Helz, R. G. Zepp, and D. G. Crosby (eds), *Aquatic and Surface Photochemistry*, CRC Press, Boca Raton, FL.

[4] H. Yao, P. Sun, D. Minakata, J.C. Crittenden, C-H. Huang, Environ. Sci. Technol. 2013, **47**, 4581.

[5] K. Li, D.R. Hokanson, J.C. Crittenden, R.R. Trussell, D. Minakata, Wat. Res. 2008, **42**, 5045.

[6] P. Westerhoff, H. Moon, D. Minakata, J.C. Crittenden, Wat. Res. 2009, **43**, 3992.

[7] L. Xing, Y. Xie, H. Cao, D. Minakata, Y. Zhang, J.C. Crittenden, C. Chemical Engineering Journal, 2014, **245**, 71-79.

[8] H. Cao, L. Xing, G. Wu, S. Xie, S.Y. Zhang, D. Minakata, J.C. Crittenden, Applied Catalysis B: Environmental., 2014, **146**, 169.

[9] G. McKay, M.M. Dong, J.L. Kleinman, S.P. Mezyk, F. Rosario-Ortiz, Environ. Sci. Technol. 2011, **45**, 6932.

[10] B.S.B. Razavi, W. Abdelmelek, W. Song, W. J. Cooper, Water Res. 2011, **45**, 625

[11] M.M. Dong, S.P. Mezyk, F.L. Rosario-Ortiz, Environ. Sci. Technol. 2010, **44**, 5714.

[12] W.J. Cooper, R.G. Zika, Science, 1983, **220**, 711.

[13] H. Herrmann, D. Hoffmann, T. Schaefer, P. Bräuer, A. Tilgner, ChemPhysChem. 2010, **11**, 3796.

[14] Coeur, C.; Jacob, V.; Foster, P. Aerosol formation from the gas-phase reaction of hydroxyl radical with the natural hydrocarbon bornyl acetate. *Atmospheric Environment*. 1999, 33(10), 1615-1620.

[15] C.C. Winterbourn, Nature Chemical Biology, 2008, **4**, 278.

[16] C. Nathan, A. Ding, Cell, 2010, **140**, 952.e1.

[17] V.B. Buxton, C.L. Greenstock, W.P. Helman, A.B. Ross, A. B. J. Phys. Chem. Ref. Data. 1988, **17**, 513.

[18] D. Minakata, K. Li, P. Westerhoff, J. Crittenden, Environ. Sci. & Technol. 2009, **43**, 6220.

[19] C. Steelink, Anal. Chem. 2002, **74**, 326A.

[20] K.M. Mostofa, C.-Q. Liu, M.A. Mottaleb, G. Wan, H. Ogawa, D. Vione, T. Yoshioka, F. Wu, In *Photobiogeochemistry of Organic Matter: Principles and Practices in Water Environments*; Mostofa, K. M. G.; Yoshioka, T.; Mottaleb, A.; Vione, D., Eds; Springer: Heidelberg 2013; pp 1-137.

[21] S. D. Richardson, T.A. Ternes, Analytical Chemistry. 2014, **86**, 2813.

[22] S.D. Snow, J. Lee, J-H. Kim, Environ. Sci. Technol. 2012, **46**, 13227.

[23] D. Minakata, J. Crittenden, Environ. Sci. & Technol. 2011, **45**, 3479.

[24] D. Minakata, W. Song, J. Crittenden, Environ. Sci. Technol. 2011, **45**, 6057.

[25] D. Minakata, S.P. Mezyk, J.W., Jones, B.R. Daws, J.C. Crittenden, Environ. Sci. Technol. 2014, **48**, 13925.

[26] T. An, Y. Gao, G. Li, P. Kamat, J. Peller, M.V. Joyce, Environ. Sci. Technol. 2014, **48**, 641.

[27] Runge E.; Gross EKU. Density-functional theory for time-dependent systems. Phys. Rev. Lett. 1984, 52, 997.

[28] M. Wielopolski, K.E. Linton, M. Marszatek, M. Gulcur, M.R. Bryce, J.E. Moser, PCCP, 2014, **16**, 2090.

[29] A.D. Laurent, C. Adamo, D. Jacquemin, Dye chemistry with time-dependent density functional theory. PCCP, 2014, **16**, 14334.

[30] D. Jacquemin, B. Mennucci, C. Adamo, PCCP, 2011, **13**, 16987.

[31] M. Zlatar, M. Gruden-Pavlović, M. Güell, M. Swart, M. PPCP, 2013, **15**, 6631.

[32] K. Whitman, S. Lyons, R. Miller, D. Nett, P. Treas, A. Zante, R. W. Fessenden, M.D. Thomas, Y. Wang, In Proceedings of the '95 Particle Accelerator Conference and International Conference on High Energy Accelerators, Dallas, Texas, May 15, 1995.

[33] W. Song, W. J. Cooper, S.P. Mezyk, J. Greaves, B.M. Peake, Environ. Sci. Technol. 2008, **42**, 1256.

[34] Gaussian 09, Revision D.02. Frisch, M. J.; Trucks, G. W.; Schlegel, H. B.; Scuseria, G. E.; Robb, M. A.; Cheeseman, J. R.; Scalmani, G.; Barone, V.; Mennucci, B.; Petersson, G. A.; Nakatsuji, H.; Caricato, M.; Li, X.; Hratchian, H. P.; Izmaylov, A. F.; Bloino, J.; Zheng, G.; Sonnenberg, J. L.; Hada, M.; Ehara, M.; Toyota, K.; Fukuda, R.; Hasegawa, J.; Ishida, M.; Nakajima, T.; Honda, Y.; Kitao, O.; Nakai, H.; Vreven, T.; Montgomery, J. A., Jr.; Peralta, J. E.; Ogliaro, F.; Bearpark, M.; Heyd, J. J.; Brothers, E.; Kudin, K. N.; Staroverov, V. N.; Kobayashi, R.; Normand, J.; Raghavachari, K.; Rendell, A.; Burant, J. C.; Iyengar, S. S.; Tomasi, J.; Cossi, M.; Rega, N.; Millam, N. J.; Klene, M.; Knox, J. E.; Cross, J. B.; Bakken, V.; Adamo, C.; Jaramillo, J.; Gomperts, R.; Stratmann, R. E.; Yazyev, O.; Austin, A. J.; Cammi, R.; Pomelli, C.; Ochterski, J. W.; Martin, R. L.; Morokuma, K.; Zakrzewski, V. G.; Voth, G. A.; Salvador, P.; Dannenberg, J. J.; Dapprich, S.; Daniels, A. D.; Farkas, Ö.; Foresman, J. B.; Ortiz, J. V.; Cioslowski, J.; Fox, D. J. Gaussian, Inc., Wallingford CT, 2009.

[35] Y. Zhao, D.G. Truhlar, Theor. Chem. Acc., **120**, 215.

[36] A. V. Marenich, C. J. Cramer, D.G. Truhlar, D.G. J. Phys. Chem. B, 2009, **113**, 6378.

[37] F. Trani, G. Scalmani, G.S. Zheng, I. Carnimeo, M. J. Frisch, V. Barone, J. Chem. Theory Comput. 2011, **7**, 3304-3313.

[38] W. Zheng, M. Andrec, E. Gallicchio, R.M. Levy, PNAS. 2007, **104**, 15340.

[39] P.L. Brezonik, Chemical Kinetics and Process Dynamics in Aqueous Systems; Lewis Publishers: Boca Raton, FL, 2002.

[40] M. von Smoluchowski, Z. Phys. Chem. 1917, **92**, 129.

[41] W. Hayduk, H. Laudie, AIChE J. 1974, **20**, 611.

[42] S. W. Benson, Thermochemical Kinetics, 2nd ed.; Wiley Interscience: New York, 1976.

[43] H. Eyring, H. Gershinowitz, C.E. Sun, J. Chem. Phys. 1935, **3**, 786.

[44] L. Ashton, G.V. Buxton, C.R. Stuart, J. Chem. Soc. Fraday Trans. 1995, **91**, 1631.

[45] R. Wander, P. Neta, L. M. Dorfman, J. Phys. Chem. 1968, **72**, 2946.

[46] B. G. Kwon, S. Ryu, J. J. Yoon, Ind. Eng. Chem. 2009, **15**, 809.

[47] T. Charbouillot, M. Brigante, G. Mailhot, P.R. Maddigapu, C. Minero, D. Vione, J. Photochem. Photobiol. A. Chem. 2011, **222**, 70.

[48] G. Mark, H-P. Schuchmann, M.B. Schuchmann, L. Prager, C. von Sonntag, Environ. Sci. Technol. 2003, **37**, 372.

[49] M. Simic, M. Z. Hoffman, M. Ebert, The Journal of Phys. Chem. 1973, **77**, 1117.

[50] J.-D. Chai, M. Head-Gordon, Phys. Chem. Chem. Phys., 2008, **10**, 6615.

[51] K.-D. Asmus, H. Möckel, A. Henglein. J. Phys. Chem. 1973, **77**, 1218-1221.

Experimental and Theoretical Studies on Aqueous-Phase Reactivity of Hydroxyl Radicals with Multiple Carboxylated and Hydroxylated Benzene Compounds

Prepared for Physical Chemistry Chemical Physics (PCCP)

Tables 1-4 and Figures 1-7

Daisuke Minakata[1*]
Weihua Song[2]
Stephen P. Mezyk[3]
William J. Cooper[4]

1. Department of Civil and Environmental Engineering, Michigan Technological University, 1400 Townsend Drive, Houghton, MI, 49931.
2. Department of Environmental Science and Engineering, Fudan University, Shanghai, P.R. China.
3. Department of Chemistry and Biochemistry, California State University Long Beach, Long Beach CA 90840.
4. Department of Civil and Environmental Engineering, University of California, Irvine, CA 92697.

*Corresponding author. dminakat@mtu.edu, 906-487-1830

Table 1

Overall experimental and calculated results for the addition of HO• to the hydroxylated and carboxylated benzene compounds including the literature reported values such as Ashton et al. (1995)[44] and Wander et al. (1968)[45] for benzoic acid, Kwon et al. (2009)[46] for benzoate and Charbouillot et al. (2011)[47] for terephthalic acid.

	$k_{HO•,exp,}$ M^{-1} s^{-1}	$\lambda_{max,\ exp}$ nm	pH	Reference	$\Delta G^{act}_{aq,calc,}$ kcal/mol	V_{calc} cm^3/molecule	k_D, $M^{-1}s^{-1}$	k_{chem}, $M^{-1}s^{-1}$
Benzoic acid	1.80×10^9			Ashton et al., 1995	1.43	87.10	1.13×10^{10}	1.80×10^9
	$(4.30 \sim 6.0)\times10^9$			Wander et al., 1968				
Benzoate	$(5.86\pm0.54)\times10^9$	330 nm	6.9	This study	-10.30	87.00	1.13×10^{10}	5.86×10^9
	2.50×10^9			Kwon et al., 2009				
Phthalic acid (1,2-Di)	$(4.98\pm0.16)\times10^9$	330 nm	6.9	This study	-7.85	122.21	1.15×10^{10}	4.98×10^9
Terephthalic acid (1,4-Di)	$(4.95\pm0.28)\times10^9$	360 nm	6.9	This study	-7.61	126.81	1.16×10^{10}	4.95×10^9
	$(4.0\pm0.1)\times10^9$			Charbouillot et al., 2011				
Trimesic acid (1,3,5-Tri)	$(3.53\pm0.35)\times10^9$	350 nm	6.9	This study	-6.12	132.70	1.16×10^{10}	3.53×10^9
Pyromellitic acid (1,2,4,5-Tetra)	$(1.27\pm0.03)\times10^9$	370 nm	6.9	This study				
(1,2,3,4,5-Penta)	$(7.55\pm0.17)\times10^8$	370 nm	6.9	This study				
Salicylic acid	$(1.07\pm0.07)\times10^{10}$	320 nm	7.0	This study	-23.4	101.823	1.14×10^{10}	1.78×10^{11}
3-hydroxybenzoic acid	$(7.27\pm0.23)\times10^9$	360 nm	7.0	This study	-16.07	113.572	1.15×10^{10}	1.99×10^{10}
4-hydroxybenzoic acid	$(8.16\pm0.50)\times10^9$	370 nm	7.0	This study	-17.74	101.769	1.14×10^{10}	2.88×10^{10}
2,3-dihydroxybenzoic acid	$(9.90\pm0.40)\times10^9$	330 nm	7.0	This study	-15.08	105.298	1.14×10^{10}	7.49×10^{10}
2,4-dihydroxybenzoic acid	$(8.43\pm0.75)\times10^9$	330 nm	7.0	This study	-15.71	115.519	1.15×10^{10}	3.17×10^{10}
2,5-dihydroxybenzoic acid	$(5.51\pm0.50)\times10^9$	300 nm	7.0	This study	-13.34	109.959	1.14×10^{10}	1.06×10^{10}
2,6-dihydroxybenzoic acid	$(8.87\pm0.70)\times10^9$	350 nm	7.0	This study	-14.26	109.234	1.14×10^{10}	3.95×10^{10}
2,3,4-trihydroxybenzoic acid	$(7.87\pm0.28)\times10^9$	380 nm	7.0	This study	-12.94	92.366	1.13×10^{10}	2.58×10^{10}
3,4,5-trihydroxybenzoic acid	$(6.33\pm0.16)\times10^9$	410 nm	7.0	This study	-16.81	120.569	1.15×10^{10}	1.41×10^{10}

Table 2

The SOMO-LUMO energy gap calculated at the level of wB97XD/cc-pVQZ and M06-2X/cc-pVQZ. Values in () are by M06-2X/cc-pVQZ. The lowest excited state with the MO contributions calculated at the level of M06-2X/cc-pVQZ for the aqueous-phase reaction of HO• with benzoate.

Compounds		Benzoate					
Position of HO attack		Ortho		Meta		Para	
		Alpha-spin	Beta-spin	Alpha-spin	Beta-spin	Alpha-spin	Beta-spin
energy, eV	SOMO-LUMO gap	8.65 (6.92)	7.97 (6.42)	8.85 (7.07)	7.7 (6.2)	8.5 (6.77)	8.37 (6.72)
Lowest excited state	λ_{exc}, nm	460		472		440	
	Energy, eV	2.7		2.63		2.82	
	f	0.0057		0.0051		0.0004	
		SOMO → LUMO (-0.486)	SOMO-3 → LUMO (0.215) SOMO → LUMO (0.832)	SOMO → LUMO (-0.404)	SOMO-3 → LUMO (0.233) SOMO-2 → LUMO (-0.101) SOMO → LUMO (0.866)	SOMO → LUMO (-0.578)	SOMO → LUMO (0.794)

Table 3

The SOMO-LUMO energy gap calculated at the level of wB97XD/cc-pVQZ and M06-2X/cc-pVQZ. Values in () are by M06-2X/cc-pVQZ. The lowest excited state with the MO contributions calculated at the level of M06-2X/cc-pVQZ for the addition of HO• to multiple carboxylated benzene compounds.

Compounds		Phthalic acid (1,2-Di)				Terephthalic acid (1,4-Di)	
Position of HO attack		3 position		4 position		2 or 3 position	
		Alpha-spin	Beta-spin	Alpha-spin	Beta-spin	Alpha-spin	Beta-spin
energy, eV	SOMO-LUMO gap	8.04 (6.57)	7.98 (6.15)	7.62 (6.61)	5.23 (3.89)	8.29 (6.34)	7.64 (6.44)
	λ, nm	490.73		1230		474.24	
Lowest	Energy, eV	2.5265		1.0079		2.61	
excited	f	0.0035		0.0008		0.0006	
state		SOMO → LUMO (0.483)	SOMO-6 → LUMO (0.111) SOMO-5 → LUMO (-0.204) SOMO → LUMO (0.824)		SOMO → LUMO (0.945) SOMO → LUMO+2 (-0.159) SOMO → LUMO+3 (0.148)	SOMO → LUMO (0.611)	SOMO-6 → LUMO (-0.192) SOMO → LUMO (0.739)

Compounds		Trimesic acid (1,3,5-Tri)		1,2,3,4,5-Penta		Pyromellitic acid	
Position of HO attack		2 or 4 position				(1,2,4,5-Tetra)	
		Alpha-spin	Beta-spin	Alpha-spin	Beta-spin	Alpha-spin	Beta-spin
energy, eV	SOMO-LUMO gap	8.31 (6.64)	7.37 (5.85)	8.51 (6.82)	7 (5.55)	8.15 (6.21)	7.35 (6.00)
	λ, nm	504.73		521		502.91	
Lowest	Energy, eV	2.4564		2.38		2.4653	
excited	f	0.01696		0.211		0.0003	
state		SOMO → LUMO (0.351)	SOMO → LUMO (-0.202) SOMO → LUMO (0.890)	SOMO → LUMO (0.287)	SOMO-15 → LUMO (0.207) SOMO → LUMO (0.917)	SOMO → LUMO (-0.577)	SOMO → LUMO (-0.201) SOMO-12 → LUMO (0.771)

Tables 4

The SOMO-LUMO energy gap calculated at the level of wB97XD/cc-pVQZ and M06-2X/cc-pVQZ. Values in () are by M06-2X/cc-pVQZ. The lowest excited state with the MO contributions calculated at the level of M06-2X/cc-pVQZ for the reactions of HO• addition to multiple hydroxylated benzoic acids

(a) Excited state energies for the reactions of HO• addition to salicylic acid at 3-, 4-, 5-, and 6-positions

Compounds		Salicylic acid (2hydroxybenzoic acid)							
Position of HO attack		3 position		4 position		5 position		6 position	
		Alpha-spin	Beta-spin	Alpha-spin	Beta-spin	Alpha-spin	Beta-spin	Alpha-spin	Beta-spin
energy, eV	SOMO-LUMO gap	8.58 (6.85)	7.71 (6.14)	8.83 (7.09)	7.89 (6.24)	8.27 (6.52)	8.05 (6.58)	8.45 (6.69)	7.86 (6.24)
	λmax	477.94		470.83		439 (449.88)		479.21	
Lowest	Energy	2.594		2.6333		2.8237 (2.7559)		2.59	
excited	f	0.0096		0.0084		0.0001 (0.0003)		0.0077	
state		SOMO → LUMO (0.431)	SOMO-3 → LUMO (-0.160) SOMO → LUMO (0.875)	SOMO → LUMO (0.361)	SOMO → LUMO (0.915)	SOMO → LUMO (-0.639)	SOMO-3 → LUMO (-0.224) SOMO → LUMO (0.708)	SOMO → LUMO (-0.460)	SOMO → LUMO (0.868)

(b) Excited state energies for the reactions of HO• addition to 3-hydroxybenzoic acid at 3-, 4-, 5-, and 6-positions

Compounds		3-hydroxybenzoic acid							
Position of HO attack		2 position		4 position		5 position		6 position	
		Alpha-spin	Beta-spin	Alpha-spin	Beta-spin	Alpha-spin	Beta-spin	Alpha-spin	Beta-spin
energy, eV	SOMO-LUMO gap	8.17 (6.42)	8.03 (6.36)	8.84 (7.10)	7.91 (6.25)	9.22 (7.44)	7.27 (5.69)	7.66 (5.94)	8.31 (6.87)
	λmax	474.39		452.89 (468.17)		544.07 (548.24)		457.6 (468.13)	
Lowest	Energy	2.6135		2.7376 (2.6483)		2.2788 (2.2615)		2.709 (2.6485)	
excited	f	0.0013		0.009 (0.0096)		0.0154 (0.0147)		0.0249 (0.0283)	
state		SOMO → LUMO (-0.583)	SOMO → LUMO (0.793)	SOMO → LUMO (-0.369)	SOMO-2 → LUMO (0.122) SOMO → LUMO (0.906)	SOMO → LUMO (0.245)	SOMO → LUMO (0.953)	SOMO → LUMO (0.871)	SOMO → LUMO (-0.454)

(c) Excited state energies for the reactions of HO• addition to 4-hydroxybenzoic acid at 2- and 3-positions and to 2,3-dihydroxybenzoic acid at 4-, 5-, and 6-positions

Compounds		4-hydroxybenzoic acid			
Position of HO attack		2 position		3 position	
		Alpha-spin	Beta-spin	Alpha-spin	Beta-spin
energy, eV	SOMO-LUMO gap	8.64 (6.88)	7.22 (5.61)	7.9 (6.21)	8.05 (6.38)
	λmax	551.1 (561.14)		464.21 (479.39)	
Lowest excited state	Energy	2.2498 (2.2095)		2.67 (2.5863)	
	f	0.0201 (0.0183)		0.0002 (0.0001)	
		SOMO → LUMO (-0.261)	SOMO → LUMO (0.948)	SOMO → LUMO (0.596)	SOMO → LUMO (0.776)

Compounds		2,3-dihydroxybenzoic acid					
Position of HO attack		4 position		5 position		6 position	
		Alpha-spin	Beta-spin	Alpha-spin	Beta-spin	Alpha-spin	Beta-spin
energy, eV	SOMO-LUMO gap	8.84 (7.11)	7.28 (5.66)	8.49 (6.75)	7.65 (6.09)	8.02 (6.31)	7.82 (6.28)
	λmax	530.68 (544.71)		483.81 (484.91)		460.66 (459.41)	
Lowest	Energy	2.3363 (2.2761)		2.5627 (2.5568)		2.6915 (2.6988)	
excited	f	0.0269 (0.0279)		0.0089 (0.0066)		0.0075 (0.0048)	
state		SOMO → LUMO (-0.191) SOMO → LUMO+1 (0.127)	SOMO → LUMO (0.959)	SOMO → LUMO (-0.387)	SOMO → LUMO (0.896)	SOMO → LUMO (0.612)	SOMO-4 → LUMO (0.113) SOMO → LUMO (0.755)

(d) Excited state energies for the reactions of HO• addition to 2,4-dihydroxybenzoic acid at 3-, 5-, and 6-positions and to 2,6-dihydroxybenzoic acid at 4- and 5-positions

Compounds		2,4-dihydroxybenzoic acid					
Position of HO attack		3 position		5 position		6 position	
		Alpha-spin	Beta-spin	Alpha-spin	Beta-spin	Alpha-spin	Beta-spin
energy, eV	SOMO-LUMO gap	7.99 (6.33)	7.83 (6.18)	7.98 (6.28)	8.09 (6.52)	8.66 (6.89)	7.29 (5.67)
Lowest	λmax	344.47 (491.16)		450.25 (461.35)		533.66 (540.13)	
excited	Energy	3.5992 (2.5243)		2.7537 (2.6874)		2.3233 (2.2955)	
state	f	0.1098 (0.0025)		0.0017 (0.0011)		0.0231 (0.0208)	
		SOMO → LUMO (0.819)	SOMO → LUMO (0.537)	SOMO → LUMO (0.689)	SOMO-2 → LUMO (0.112) SOMO → LUMO (0.685)	SOMO → LUMO (0.275)	SOMO → LUMO (0.945)

Compounds		2,6-dihydroxybenzoic acid			
Position of HO attack		4 position		5 position	
		Alpha-spin	Beta-spin	Alpha-spin	Beta-spin
energy, eV	SOMO-LUMO gap	9.28 (7.53)	3.04 (5.36)	8.08 (6.39)	8.06 (6.54
Lowest	λmax	595.43 (601.53)		442.98 (448.87)	
excited	Energy	2.0823 (2.0611)		2.7988 (2.7621)	
state	f	0.0233 (0.0229)		0.0033 (0.0034)	
		SOMO → LUMO (0.171)	SOMO → LUMO (0.970)	SOMO → LUMO (0.712)	SOMO-2 → LUMO (0.135) SOMO → LUMO (0.656)

(e) Excited state energies for the reactions of HO• addition to 2,5-dihydroxybenzoic acid at 3-, 4-, and 6-positions and to 3,4-dihydroxybenzoic acid at 2- and 5-positions

Compounds		2,5-dihydroxybenzoic acid					
Position of HO attack		3 position		4 position		6 position	
		Alpha-spin	Beta-spin	Alpha-spin	Beta-spin	Alpha-spin	Beta-spin
energy, eV	SOMO-LUMO gap	9 (7.28)	7.32 (5.72)	9.04 (7.30)	7.37 (5.76)	8.64 (6.90)	7.38 (5.79)
Lowest	λmax	528.18 (529.77)		522.92 (523.92)		518.23 (519.41)	
excited	Energy	2.3474 (2.3404)		2.371 (2.3665)		2.3924 (2.487)	
state	f	0.019 (0.0181)		0.0143 (0.0133)		0.024 (0.0196)	
		SOMO → LUMO (-0.251)	SOMO → LUMO (0.952)	SOMO → LUMO (0.234)	SOMO → LUMO (0.953)	SOMO → LUMO (-0.302)	SOMO → LUMO (0.934)
Compounds		3,4-dihydroxybenzoic acid					
Position of HO attack		2 position		5 position		6 position	
		Alpha-spin	Beta-spin	Alpha-spin	Beta-spin	Alpha-spin	Beta-spin
energy, eV	SOMO-LUMO gap	8.57 (6.82)	7.21 (5.59)	8.28 (6.56)	7.45 (5.81)	7.69 (5.98)	8.35 (6.75)
Lowest	λmax	552.15 (568.52)		525.74 (543.49)		457.47 (469.36)	
excited	Energy	2.2455 (2.1808)		2.3583 (2,2813)		2.7102 (2.6415)	
state	f	0.025 (0.0236)		0.0142 (0.0137)		0.0216 (0.0257)	
		SOMO → LUMO (0.265)	SOMO → LUMO (0.949)	SOMO → LUMO (0.316)	SOMO → LUMO (0.930)	SOMO → LUMO (0.867)	SOMO → LUMO (0.458)

(f) Excited state energies for the reactions of HO• addition to 2,3,4-trihydroxybenzoic acid at 5- and 6-position, and to 3,4,5-trihydroxybenzoic acid at 2- or 6-position

Compounds		2,3,4-trihydroxybenzoic acid				3,4,5-trihydroxybenzoic acid	
Position of HO attack		5 position		6 position		2 or 6 position	
		Alpha-spin	Beta-spin	Alpha-spin	Beta-spin	Alpha-spin	Beta-spin
energy, eV	SOMO-LUMO gap	8.38 (6.68)	7.72 (6.14)	8.39 (6.69)	7.51 (5.60)	7.74 (6.09)	7.93 (6.32)
Lowest	λmax	457.78 (469.08)		494.38 (480.47)		462.79 (469.71)	
excited	Energy	2.6505 (2.6432)		2.5079 (2.5805)		2.6791 (2.6396)	
state	f	0.0033 (0.0037)		0.0091 (0.0059)		0.0044 (0.0049)	
		SOMO → LUMO (0.427) SOMO → LUMO+1 (0.143)	SOMO → LUMO (0.871)	SOMO → LUMO (0.353)	SOMO → LUMO (0.916)	SOMO → LUMO (0.705)	SOMO → LUMO (-0.679)

Figure 1

Linear Free Energy Relationships between experimental rate constants for the chemical reactions, k_{chem}, and theoretically calculated $\Delta G^{act}_{aq,calc}$. The error bar indicates the range of the literature reported values.

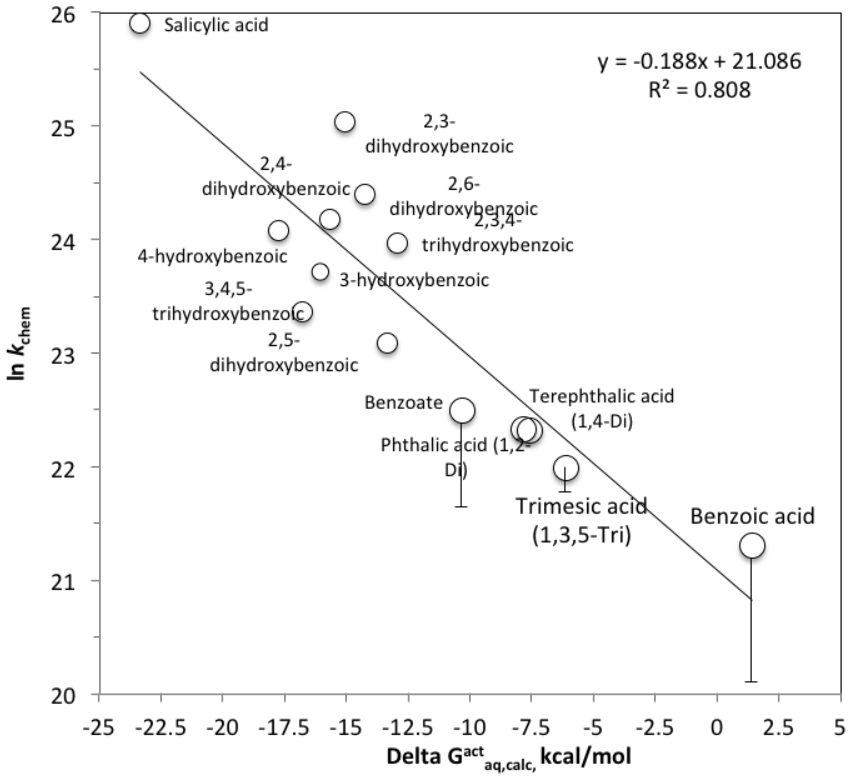

Figure 2

Experimental transient absorption spectra for the reaction of HO• with benzoate

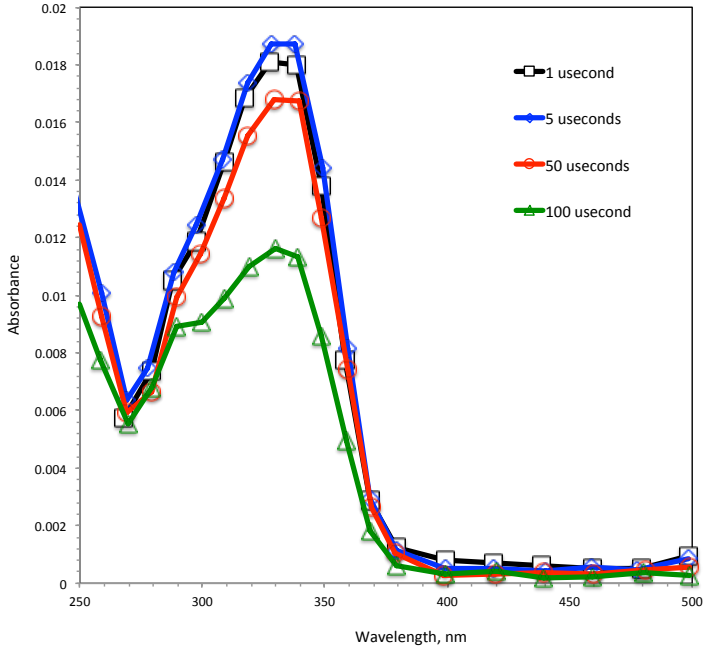

Figure 3

Molecular orbitals of SOMO-1, SOMO, LUMO, and LUMO+1 for the aqueous-phase reaction of HO• with benzoate

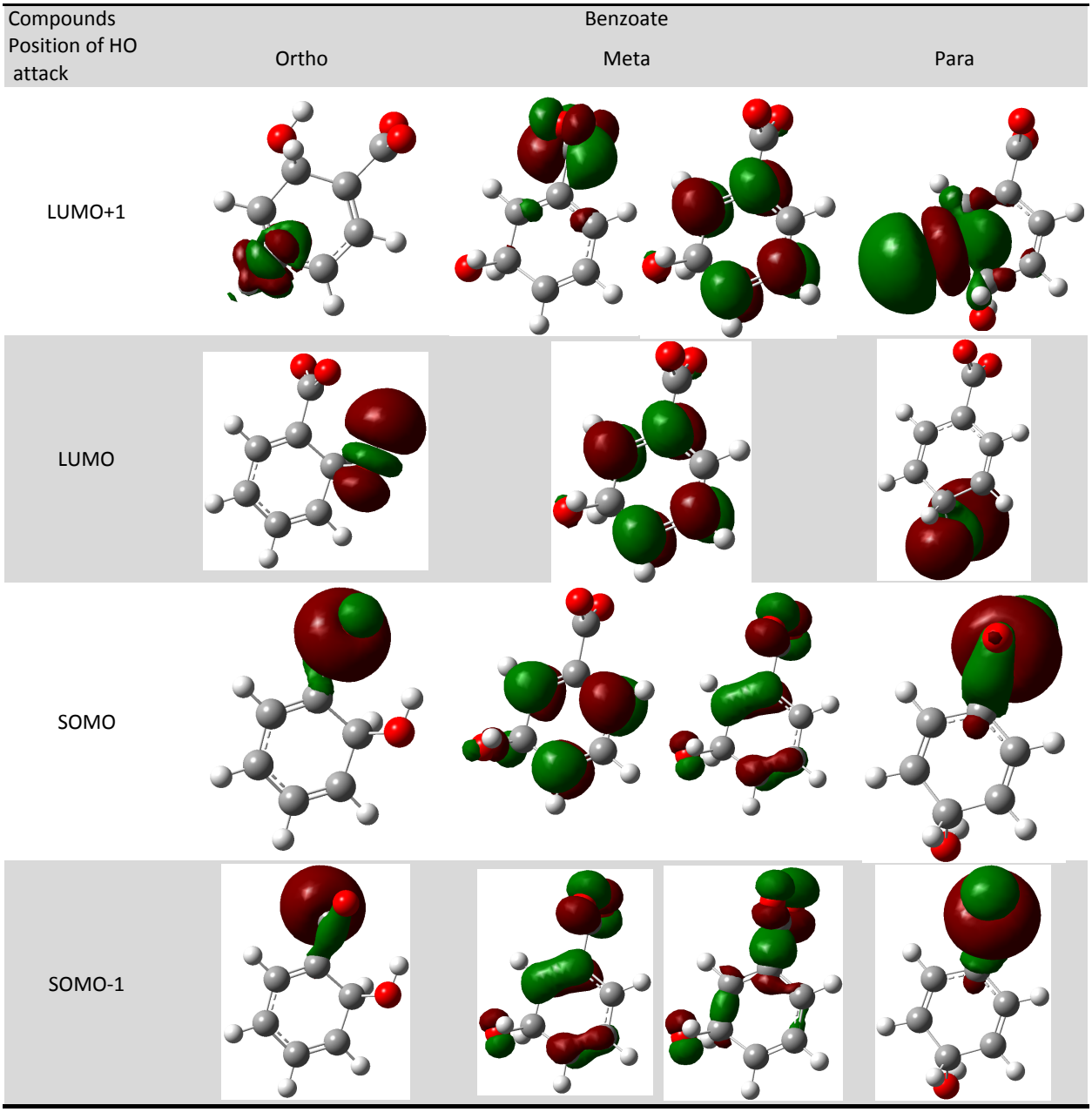

Figure 4

Experimental transient spectra for the addition of HO• to multiple carboxylated benzene compounds

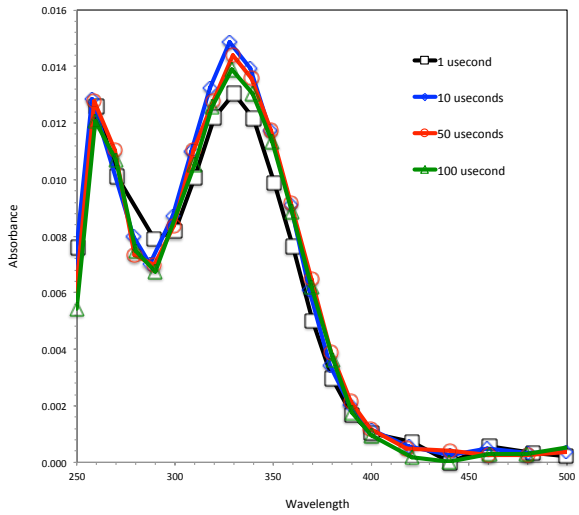

(a) Phthalic acid

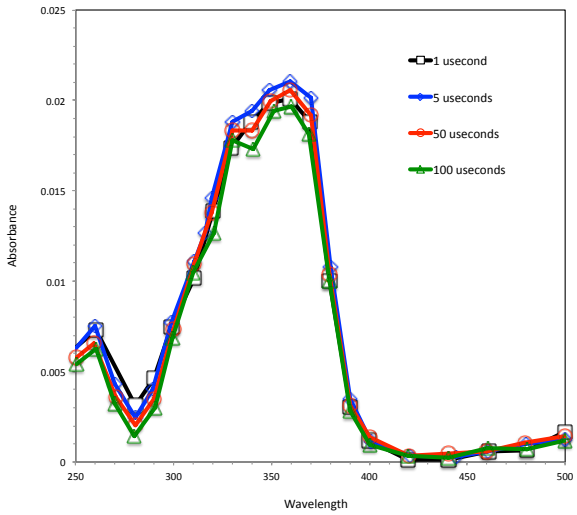

(b) Terephthalic acid

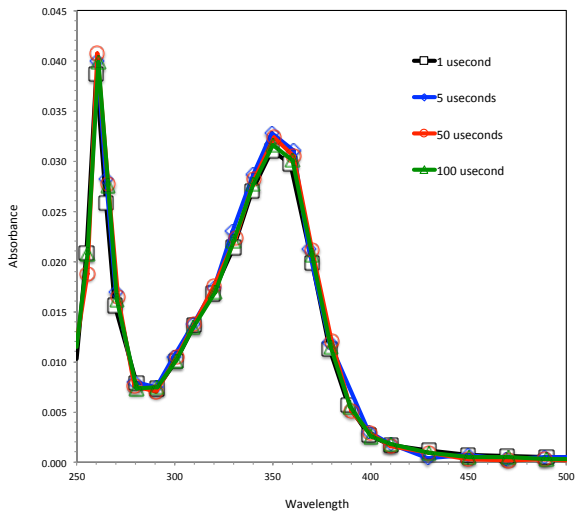

(c) Trimesic acid

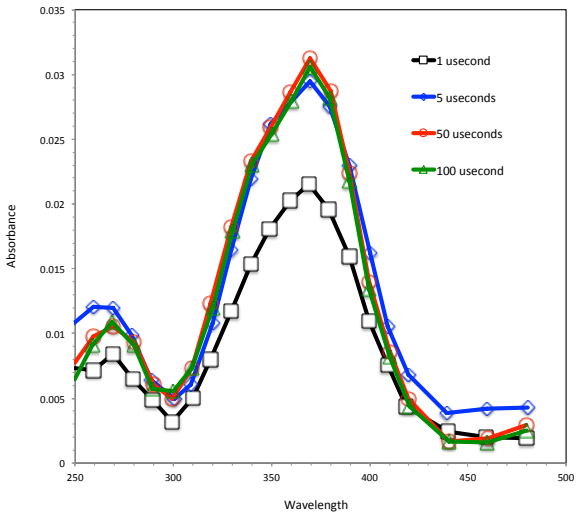

(d) Pyromellitic acid

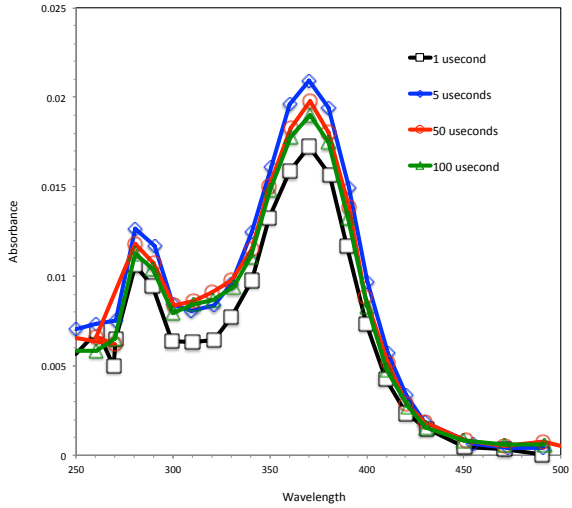

103

104 (e) 1,2,3,4,5-Pentacarboxylic acid

105

106

Figure 5

Theoretically calculated MOs for the addition of HO• to multiple carboxylated benzene compounds

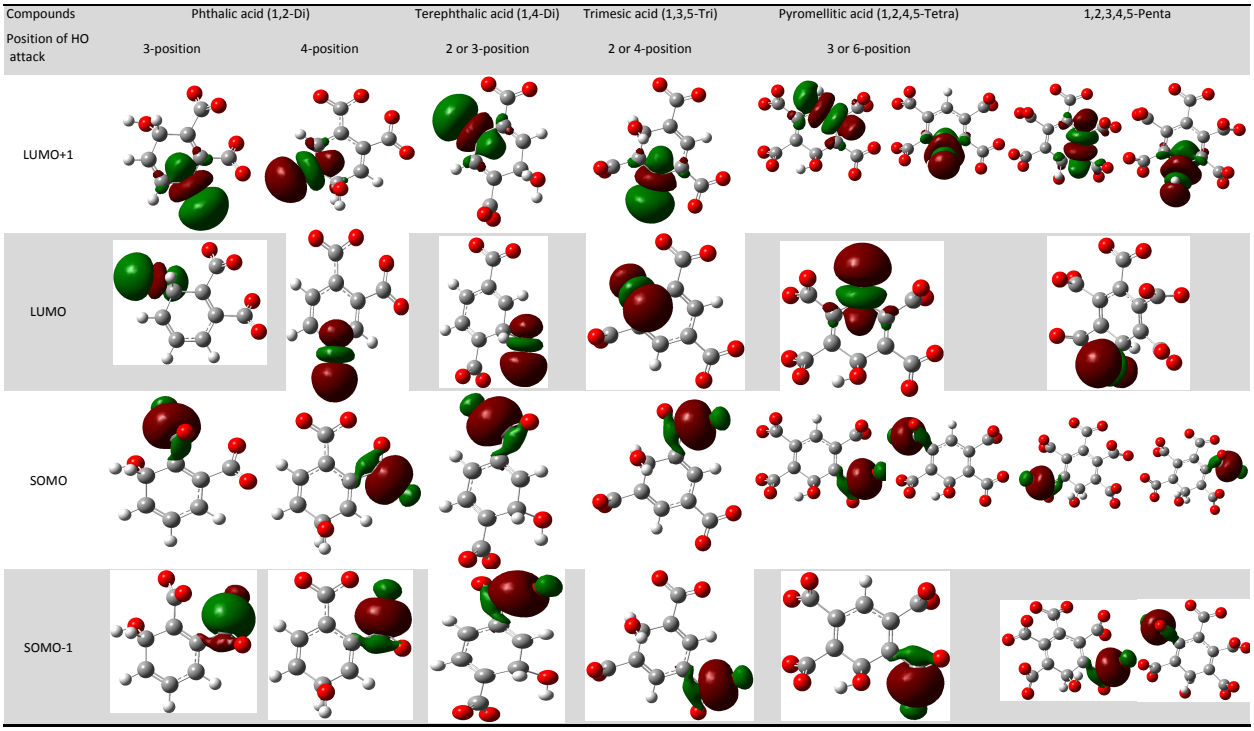

Figure 6

Time-dependent transient spectra for the reaction of HO• with multiple hydroxylated benzoic acids

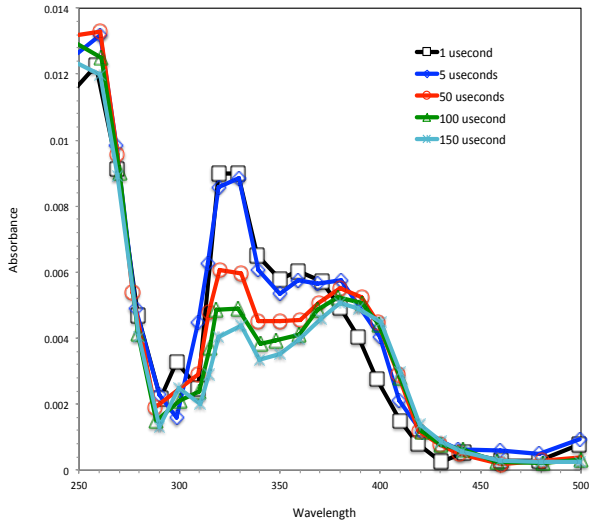

(a) Salicylic acid

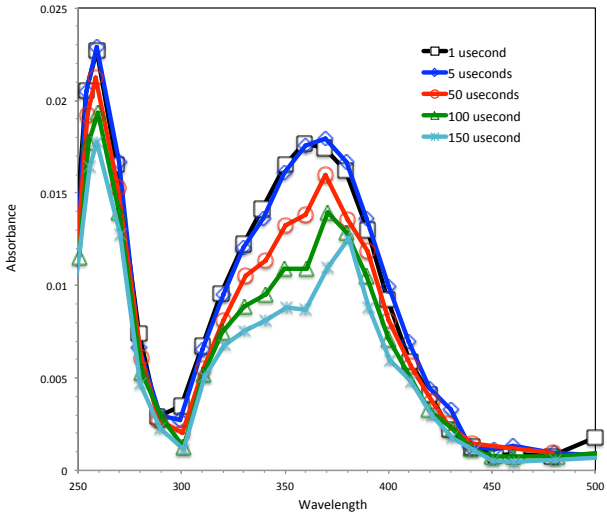

(b) 3-hydroxybenzoic acid

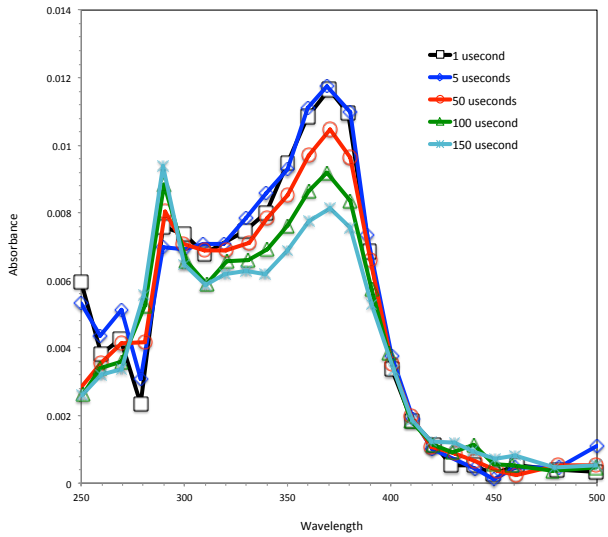

(c) 4-hydroxybenzoic acid

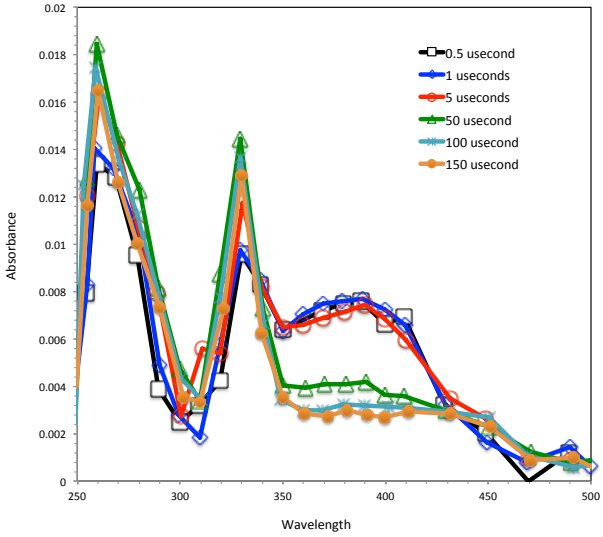

(d) 2,3-dihydrobenzoic acid

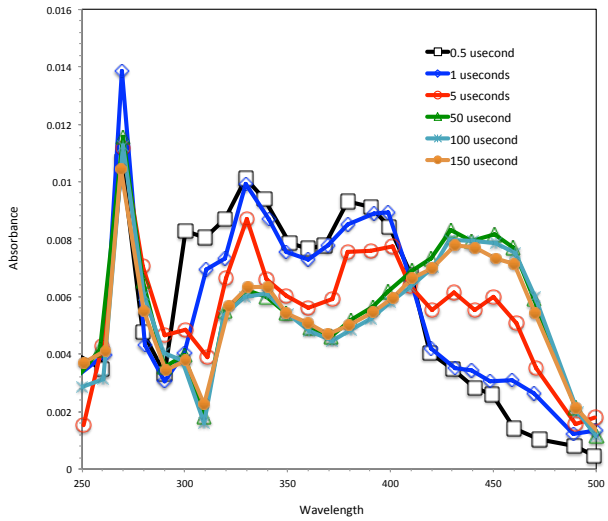

(e) 2,4-dihydrobenzoic acid

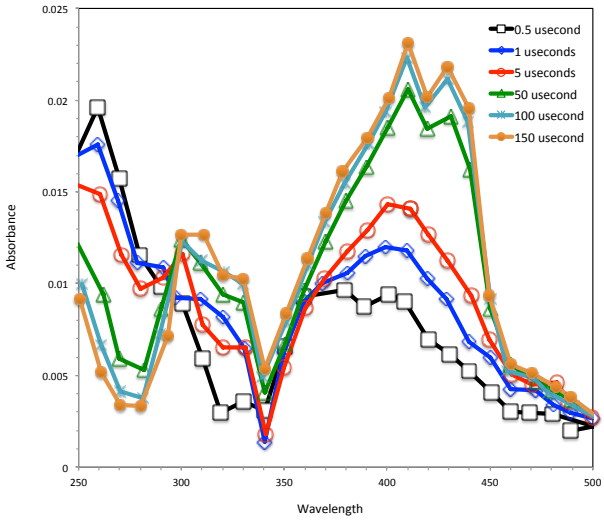

(f) 2,5-dihydrobenzoic acid

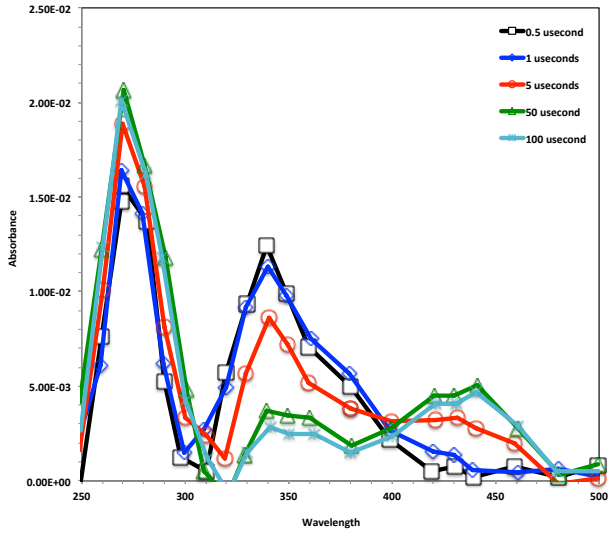

(g) 2,6-dihydrobenzoic acid

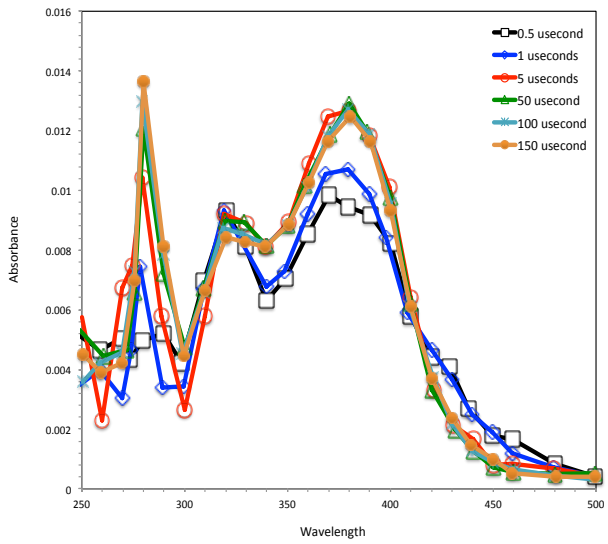

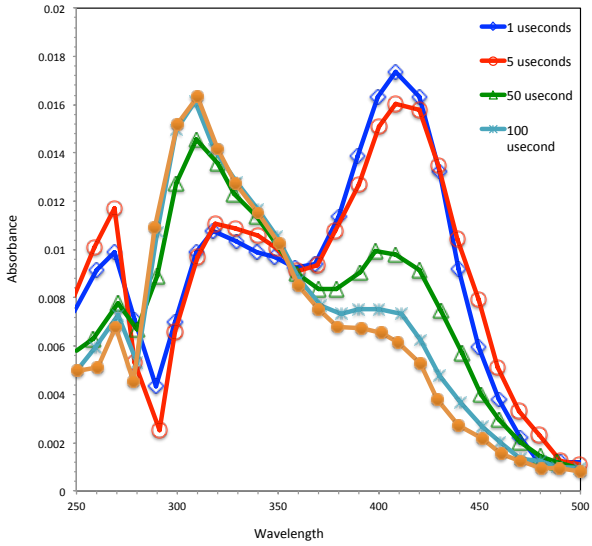

122

123 (h) 2,3,4-trihydrobenzoic acid (i) 3,4,5-trihydrobenzoic acid

124

125

Figure 7

Theoretically calculated MO for the addition of HO• to the salicylic acid

Compounds Position of HO• attack	Salicylic acid			
	3-possition	4-position	5-position	6-position
LUMO+1	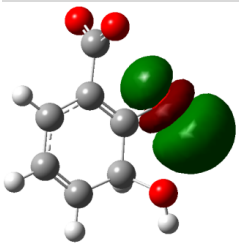	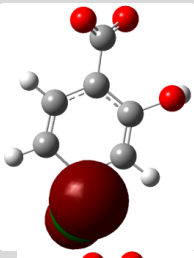	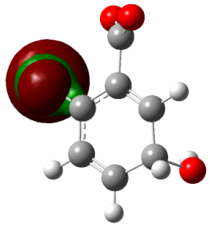	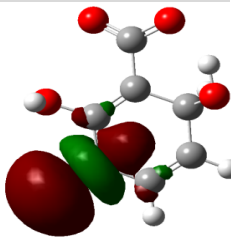
LUMO	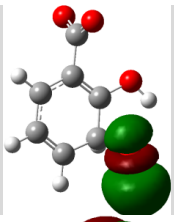	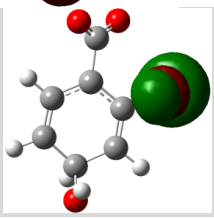	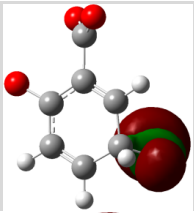	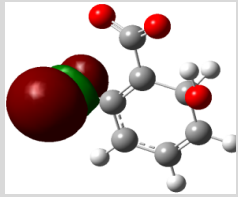
SOMO	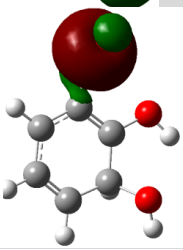	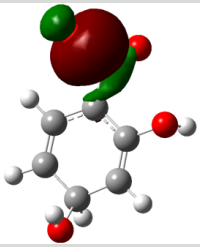	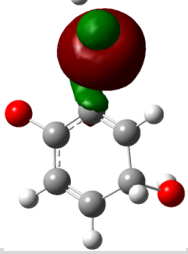	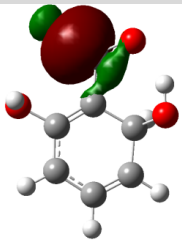
SOMO-1